RSC Advances

PAPER

View Article Online
View Journal | View Issue

Cite this: *RSC Adv.*, 2020, **10**, 39348

Ultrasound-mediated delivery of RGD-conjugated nanobubbles loaded with fingolimod and superparamagnetic iron oxide nanoparticles: targeting hepatocellular carcinoma and enhancing magnetic resonance imaging†

Xin-Min Guo, * Jia-Lin Chen, Bao-Hui Zeng, Ji-Chuang Lai, Cui-Yan Lin and Mei-Yan Lai

Nanobubbles (NBs) are considered to be a new generation of ultrasound-responsive nanocarriers that can effectively target tumors, accurately release multi-drugs at desired locations, as well as simultaneously perform diagnosis and treatment. In this study, we designed theranostic NBs (FTY720@SPION/PFP/RGD-NBs) composed of RGD-modified liposomes as the shell, and perflenapent (PFP), superparamagnetic iron oxide nanoparticles (SPION), and fingolimod (2-amino-2[2-(4-octylphenyl)ethyl]-1,3-propanediol, FTY720) encapsulated as the core. The prepared FTY720@SPION/PFP/RGD-NBs were black spheres with a diameter range of 160–220 nm, eligible for enhanced permeability and retention (EPR) effects. The calculated average drug loading efficiency (LE) and encapsulation efficiency (EE) of the FTY720@SPION/PFP/RGD-NBs were 9.18 ± 0.61% and 88.26 ± 2.31%, respectively. With the promotion of low-intensity focused ultrasound (LIFU), the amount and the rate of FTY720 released from the prepared NB complex were enhanced when compared to the samples without LIFU treatment. *In vitro* magnetic resonance imaging (MRI) trials showed that the prepared FTY720@SPION/PFP/RGD-NBs had a high relaxation rate and MRI T2-weighted imaging (T2WI) scanning sensitivity conditions. The cell viability studies demonstrated that both HepG2 and Huh7 cells co-cultured with FTY720@SPION/PFP/RGD-NB (100 μg mL^{-1}) + LIFU treatment had the lowest survival rate compared with the other groups at 24 h and 48 h, showing that FTY720@SPION/PFP/RGD-NB had the strongest anti-tumor efficiency among the prepared NBs. The cytotoxicity study also demonstrated that the prepared NBs had low toxicity to normal fibroblast 3T3 cells. Cellular uptake studies further indicated that both LIFU treatment and RGD modification could effectively improve the tumor-targeted effects, thereby enhancing the antitumor efficacy. The qRT-PCR results indicated that LIFU-mediated FTY720@SPION/PFP/RGD-NB could significantly cause the activation of Caspase3, Caspase9 and p53 compared to the control group, inducing HepG2 apoptosis. These results together indicated that FTY720@SPION/PFP/RGD-NBs combined with LIFU may serve as a multifunctional drug delivery platform for hepatocellular carcinoma treatment and provide a new strategy for tumor visualization by MRI.

Received 23rd July 2020
Accepted 11th October 2020

DOI: 10.1039/d0ra06415g

rsc.li/rsc-advances

1. Introduction

Hepatocellular carcinoma (HCC) is one of the most malignancies in the world, and the incidence of HCC is rising every year. At present, the clinical treatment methods for HCC mainly include surgical resection, transplantation, local ablation, intervention, radiotherapy, and chemotherapy.[1,2] The insidious onset and rapid development of HCC are often accompanied by the metastasis of cancer cells inside and/or outside the liver, which brings great challenges to the diagnosis and treatment of HCC at the early stage.[3–5] Therefore, the development of drug delivery platforms that effectively target tumors, accurately release multi-drugs at desired locations, as well as simultaneously perform diagnosis and treatment has become the focus of cancer research in recent years.

Ultrasound-targeted microbubble destruction (UTMD) technology has received increasing attention in cancer treatment applications.[6–10] Microbubbles (MBs, 1–4 μM) are spherical shells made of various materials that encapsulate gas (*e.g.* perflenapent, PFP) used as ultrasonic contrast agents, playing

Department of Ultrasound, Guangzhou Red Cross Hospital, Medical College, Jinan University, 396 Tongfu Middle Road, Guangzhou, Guangdong 510220, P. R. China. E-mail: Guoxm1509257@163.com

† Electronic supplementary information (ESI) available. See DOI: 10.1039/d0ra06415g

a vital role in the ultrasound diagnosis of many diseases.[11,12] Recent studies have shown that the UTMD carrier can target the drug and gene to local tumor tissues, and then destroy the microbubble structure to release the drug under specific ultrasonic irradiation.[9,13–15] UTMD can cause a series of changes in the cell structure and function of target tissues, increase pores on the cell surface, enhance permeability of tissues and cells, and improve phagocytic capacity of cells, thereby promoting the targeted delivery and therapeutic efficacy of the agents into cells.[16–19] However, the size of MBs limits their mobility to penetrate the tumor blood vessel wall (the gap between 380 nm and 780 nm). Therefore, nanobubbles (NBs) are considered to be a new generation of ultrasound-responsive nanocarriers that can improve the drug delivery performance both *in vitro* and *in vivo*. NBs can move from the blood vessels and enter the surrounding tissues, thereby improving the efficiency of delivery and local localization.[20–22] Similar to MBs, NBs can also be used as cavitation nuclei, causing sound pore effects through UTMD, resulting in instantaneous pore formation of biofilms and changing cell permeability. Liufu *et al.* prepared the NBs sensitive to acoustic response and glutathione (GSH), using polyethylene glycol-disulfide bond-polyethylenimine (PSP).[23] Their study showed that the UTMD technology combined with the NBs effectively promoted the deliver efficacy of ALDH1 shRNA, promoting apoptosis of ovarian cancer stem cells.[23] Sun and colleagues designed sinoporphyrin sodium (DVDMS, sonosensitizer and photosensitizer)-loaded iRGD-modified liposomes that are used for glioma therapy.[8] Through UTMD, the prepared liposomes (round 110–130 nm) could penetrate the blood–brain barrier (BBB), enhance the accumulation of DVDMS in the glioma tissue, increase reactive oxygen species (ROS) generation, and show strong antitumor efficacy both *in vitro* and *in vivo*.[8]

The use of micro- or nano-ultrasonic contrast agents in combination with other contrast agents can achieve multimodal imaging, which has become a future trend in the diagnosis and treatment of various diseases. Although ultrasound is a real-time, non-invasive imaging mode, its resolution on soft tissues is worse than magnetic resonance imaging (MRI). Feshitan *et al.* synthesized the Gd(III)-bound MBs, which could be used to measure the cavitation events during MRI-guided focused ultrasound therapy and tracked the biodistribution of shell residues.[24] Li *et al.* developed Fe_3O_4-embedded MBs as the contrast agent for both ultrasonography and MRI, and their results indicated that the shell structure plays a key role in influencing the imaging quality.[25] Yang *et al.* utilized PLA and PVA double-layered shells to prepare the MBs (3.98 μm) loading with superparamagnetic iron oxide nanoparticles (SPIONs, 12 nm), which showed a great potential to serve as double contrast agents in the applications of ultrasonography and MRI.[26] Their study demonstrated that the prepared SPIONs/MBs could be manipulated instantaneously and locally *in vivo via* cavitation by ultrasound irradiation, and the dynamic MR susceptibilities imaging technique was used to monitor these *in vivo* contrast changes.[26]

Fingolimod (2-amino-2[2-(4-octylphenyl)ethyl]-1,3-propanediol, FTY720) is a new type of immunosuppressive agent suppressing the homing of lymphocytes, which has been used in the clinical treatment of immune rejection after organ transplantation. FTY720 can be phosphorylated *in vivo* and become an analogue of sphingosine-1-phosphate (S1P), which competitively binds to S1P receptor 1 on the surface of cell membranes, inhibiting the role of S1P.[27,28] A number of studies have further demonstrated that non-phosphorylated FTY720 can inhibit the SK1 signaling pathway, as well as interfered with multiple intracellular oncogenic signaling pathways related to cancer development, resulting in strong anti-tumor and anti-metastatic effects against different types of cancers such as HCC, leukemia, breast cancer, prostate cancer, and bladder cancer.[29–34] However, the administration of FTY 720 at high doses might cause serious cardiovascular effects by its interaction with S1P receptors.[35,36] A well-designed NB drug delivery platform equipped with tumor-targeting agents (*e.g.* ligands or peptides) can effectively load and transport therapeutic drugs to the lesion areas, providing new strategies to solve the problem. Combined with the UTMD technology, the customized drug delivery platforms can greatly enhance the accumulation of drugs in the tumor tissues rather than in the normal cells, reducing the side effects and toxicity of the drugs.[6,8,21,22]

In this study, we designed theranostic NBs (FTY720@SPION/PFP/RGD-NBs) composed of RGD-modified liposomes as the shell, and PFP, SPION, and FTY720 encapsulated as the core. The physiochemical properties of the prepared multifunctional drug carrier at nanoscale were characterized. The drug release and imaging effect *in vitro* under low-intensity focused ultrasound (LIFU) conditions were studied. The *in vitro* cytotoxicity, cellular uptake and cancer-related gene expression levels of various prepared NBs were investigated against HCC cells. The proposed multifunctional FTY720@SPION/PFP/RGD-NBs showed the following features: (I) effective HCC active-targeting with the assistance of LIFU; (II) enhanced EPR effects due to the nanoscale of NBs, when compared with MBs; and (III) noninvasive and real-time imaging diagnosis using MRI.

2. Materials and methods

Materials

The chemicals 1,2-distearoyl-*sn*-glycero-3-phosphoethanolamine-*N*-[maleimide(polyethylene glycol)] (DSPE-PEG2000-MAL) and 1,2-dipalmitoyl-*sn*-glycero-3-phosphocholine (DPPC) were purchased from Avanti Polar Lipids (Alabaster, Alabama, USA). Perflenapent (PFP) was supplied by Sonus Pharmaceuticals (Bothell, WA, USA). FTY720 was obtained from Selleck Chemicals (Shanghai, China). cRGDfK was synthesized by Hangzhou Peptide Biochem Co., Ltd. (Hangzhou, China, 97%). Manganese(II) acetylacetonate ($MnC_{15}H_{21}O_6$, 98%) and iron(III) acetylacetonate ($C_{15}H_{21}FeO_6$, 98%) were purchased from Macklin reagent Co., Ltd (Shanghai, China). *N*-Hydroxysuccinimide (NHS, 99%), 1-(3-dimethylaminopropyl)-3-ethylcarbodiimide hydrochloride (EDC, 99%), and 2-morpholino-ethanesulfonic acid (MES) were purchased from Aladdin reagent Co., Ltd. (Shanghai, China). DAPI and Cy5.5-NHS ester were purchased from Thermo Fisher GE Healthcare

(Buckinghamshire, UK). All reagents and solvents were of analytical grade and used without further purification unless specified.

HCC cells (HepG2 and Huh7 cells) and fibroblast NIH 3T3 cells were obtained from the Chinese Academy of Sciences (CAS, Shanghai, China). The cells were cultured in DMEM supplemented with 10% FBS and 100 U mL^{-1} penicillin–streptomycin at 37 °C in a humidified incubator with 5% CO_2.

Preparation and characterization of NBs

SPIONs were prepared as described previously.[37,38] Briefly, $C_{15}H_{21}FeO_6$ (2 mmol), $MnC_{15}H_{21}O_6$ (1 mmol) and 1,2-hexadecandiol (10 mmol) were mixed. Then, oleic acid (3 mmol), oleylamine (3 mmol) and dibenzyl ether (10 mL) were added into the reaction vessel, stirred and heated to 200 °C for 2 h, and then heated to 300 °C and refluxed for 0.5 h. After cooling to room temperature, ethanol (40 mL) was added into the reaction product and centrifuged (5500*g*, 10 min) to obtain the brown-black precipitate. After removing the supernatant, oleic acid (0.05 mL) and oleamide (0.05 mL) were added to the precipitate, and the mixture was dissolved and dispersed with *n*-hexane, followed by centrifugation (5500*g*, 10 min) to remove the undispersed residues. The obtained product (supernatant from last step) was precipitated in ethanol and centrifuged (5500*g*, 10 min) to remove the solvent, and the final product (SPION) was dispersed in *n*-hexane for preservation.

The drug-loaded liposomes FTY720@SPION/PFP/NBs were synthesized by a thin-film hydration method. Briefly, DPPC (30 mg), DSPE-PEG-MAL (15 mg) and FTY720 (10 mg) were dissolved in tetrahydrofuran (10 mL) and added into a round-bottom flask. After the powders were completely dissolved, SPIONs (25 mg mL^{-1} @ 100 μL) were added and stirred at room temperature for 1 h, then the solvent was evaporated at 40 °C for 2 h using a rotary evaporator under vacuum. Phosphate buffered saline (5 mL, pH7.4) was added to the flask, and the flask was sonicated to obtain a brown suspension. The suspension was transferred into a 20 mL epoxide tube, and PFF (200 μL) was then slowly added. An ultrasonic pulverizer (200 W, 4s–4s) was used to emulsify the suspension in the EP tube for 20 min under ice bath. The obtained product was dialyzed (MWCO = 3500) with distilled water for 3 days and then stored at −4 °C to obtain FTY720@SPION/PFP/NBs.

The target drug-loaded liposomes FTY720@SPION/PFP/RGD-NBs were prepared as follows. FTY720@PFP/Fe_3O_4/lipid NPs (10 mg mL^{-1} @ 10 mL), EDC (50 mg) and NHS (25 mg) were mixed under stirring at 37 °C for 30 min. The RGD peptide was then added into the solution and stirred magnetically at 4 °C for 8 hours. The obtained product was dialyzed (MWCO = 3500) with distilled water for 3 days and then stored at −4 °C to obtain FTY720@SPION/PFP/RGD-NBs.

The structure of SPIONs was characterized using an X-ray diffractometer (XRD) (D/Max-2550, Rigaku Inc., Japan). The magnetization properties of the prepared SPIONs and FTY720@SPION/PFP/RGD-NBs were analyzed using a vibrating sample magnetometer (VSM7407, Lake Shore Cryotronics, Inc., USA). The morphological properties of SPIONs and NB complex were examined using a transmission electron microscope (TEM) (H-800, Hitachi, Japan). The size and zeta potential of FTY720@SPION/PFP/RGD-NBs were detected by dynamic light scattering (DLS) using a Nano Zetasizer (Malvern Instruments Ltd., UK).

To measure the encapsulation efficiency (EE) and loading efficiency (LE) of the FTY720 in the FTY720@SPION/PFP/RGD-NBs, a certain amount of FTY720@SPION/PFP/RGD-NBs were subjected to centrifugation (12 000*g*, 15 min). The supernatant was collected for absorbance measurement using a UV-Vis spectrophotometer at a wavelength of 220 nm. The concentration of FTY720 was determined with a standard curve according to the Beer–Lambert law. The LE and EE were calculated using eqn (1) and (2).

$$\mathrm{EE}(\%) = \frac{\text{amount of FTY720 in the NBs}}{\text{amount of feeding FTY720}} \times 100\% \quad (1)$$

$$\mathrm{LE}(\%) = \frac{\text{amount of FTY720 in the NBs}}{\text{amount of the NBs}} \times 100\% \quad (2)$$

To measure the stabilities of FTY720@SPION/PFP/RGD-NBs, the prepared NB complex was dispersed into a PBS solution, and then divided into 2 groups, which were stored at 4 °C and 20 °C, respectively. The size distribution and PDI of NBs under both conditions were measured every day for 7 days.

In vitro release of FTY 720 from FTY720@SPION/PFP/RGD-NBs

The *in vitro* release profiles of FTY 720 from FTY720@SPION/PFP/RGD-NBs under different low-intensity focused ultrasound (LIFU) conditions were evaluated by a dialysis method. The samples of FTY720@SPION/PFP/RGD-NBs were divided into four groups (1 mL per group) and then placed into four dialysis membrane bags (MW of 3500 Da). The sealed dialysis bags were immersed in 50 mL PBS (pH 7.4) and shaken at 100 rpm at 37 °C. After 1 h, the samples treated with LIFU were performed using a SP100 sonoporator (Sonidel Ltd, United States) at a frequency of 1 MHz and a duty cycle of 50% for 60 s. At different time intervals, 1 mL samples of different groups were taken out for FTY720 amount measurements using a UV spectrophotometer at 220 nm, and an equal volume of PBS was replenished into the solution.

In vitro MRI experiments

According to the concentration of SPION concentration in the samples as 0.067 mM, 0.135 mM, 0.27 mM, 0.54 mM, and 1.08 mM, a series of FTY720@SPION/PFP/RGD-NBs in PBS solutions were prepared. The samples (1.5 mL per tube) were scanned using a 3T magnetic resonance scanner (Philips Achieva, Best, Netherlands) at room temperature. The MRI scan sequence includes T2WI and T2 mapping. The T2WI parameters are as follows: TR/TE = 2600 ms/100 ms; flip angle = 90°; NA (number of acquisitions) = 6; acquisition matrix = 384 × 305; FOV (field of view) = 80 mm × 80 mm; slice thickness = 2 mm; slice gap = 2 mm. T2 mapping used single-layer, multi-

echo self-selected echo sequence scanning, and the parameters are as follows: TR = 1500 ms; TE = 0, 20, 40, …, 160 ms; NA = 3; acquisition matrix = 176 × 123 mm; FOV = 80 mm × 80 mm; slice thickness = 1.5 mm; slice gap = 1.5 mm. According to the scanned MRI T2 map, the transverse relaxation time T_2 of each SPION concentration was obtained, and linear fitting was performed to calculate the transverse relaxation rate R_2 of the SPION sample.

Cell viability analysis

The CCK-8 assay was used to analyze the cytotoxicity of the prepared NBs complex at different concentrations (10, 25, 50 and 100 μg mL^{-1}) against HepG2, Huh7 and 3T3 cells. Briefly, cells were cultured in a 96-well plate at a concentration of 1 × 10^4 cells per well at 37 °C. After 24 h, cells were treated with PBS and various NB complexes at different concentrations at 37 °C. The selected wells (*i.e.* samples treated with FTY720@SPION/PFP/NB or FTY720@SPION/PFP/RGD-NB) were subjected to ultrasound for 60 s using a SP100 sonoporator with a frequency of 1 MHz, an ultrasound power density of 2.4 W cm^{-2} and a duty cycle of 50% (pulse frequency = 100 Hz). After 24 h, the CCK-8 solution was added into each well and incubated for 2 h at 37 °C. Cells treated with PBS solution were used as a blank control. The absorbance of each sample well was measured at 450 nm using a microplate reader (Thermo Fisher Scientific, USA). All the measurements were repeated three times. The cell viability was calculated using eqn (3):

$$\text{Cell viability}(\%) = \frac{\text{OD value of the sample}}{\text{OD value of the blank}} \times 100\% \quad (3)$$

Cellular uptake of the prepared NBs complex by HepG2 cells *in vitro*

HepG2 cells (1 × 10^5 cells per well) were cultured in a glass-bottomed Petri dish and incubated at 37 °C for 24 h. Cells were then treated with a fresh medium containing cy5.5-labeled FTY720@SPION/PFP/NBs or FTY720@SPION/PFP/RGD-NBs. Two of four groups were subjected to LIFU treatment for 60 s (power of 2.4 W cm^{-2}, a duty cycle of 50% and a pulse frequency of 100 Hz). All the samples were then incubated at 37 °C in darkness for 1 h and washed three times with PBS before fixing with 4% paraformaldehyde at room temperature for 15 min. DAPI was added to the samples to stain the cell nuclei in darkness for 20 min. Cell samples were washed twice with PBS and visualized using a confocal-laser scanning microscope (CLSM) (FV10i, Olympus Corporation, Japan). The nuclei of cells were indicated in blue and the NB complex in red.

MRI (1.5T scanner, Philips, Best, Netherlands) was also used to monitor the cellular uptake efficiency of the prepared NBs *in vitro*. Briefly, HepG2 cells (1 × 10^4 cells per well) were cultured in 96-well plates at 37 °C. After 24 h, the culture media were removed and the cells were treated with fresh media containing FTY720@SPION/PFP/NBs or FTY720@SPION/PFP/RGD-NBs. Two of the four groups were subjected to LIFU treatment for 60 s (power of 2.4 W cm^{-2}, a duty cycle of 50% and a pulse frequency of 100 Hz). All the samples were incubated at 37 °C for 1 h. Then, the cells were washed three times with PBS, centrifuged, and resuspended in PBS containing 0.5% agarose in 96-well plates for the MRI test.

Quantitative real-time-polymerase chain reaction analysis

Quantitative reverse transcription-polymerase chain reaction (qRT-PCR) was used to examine the effects of HepG2 co-cultured in the presence of the prepared NBs for 48 h with or without LIFU treatment on the expression levels of Caspase-9, Caspase-3 and p53. The primer sequences used for PCR amplification are listed in Table 1, and all primers were provided by RIBOBIO Co. Ltd. (Guangzhou, China). All experiments were performed in triplicate.

Statistical analysis

All measurements were carried out in triplicate, and the data are expressed as mean ± standard deviation (SD). Statistical analysis was performed using the SPSS 20.0 software (IBM Corp., NY, USA). The results with p-values less than 0.05 ($p < 0.05$, *) were considered statistically significant, while results with p-values less than 0.01 ($p < 0.01$, **) were considered highly significant.

3. Results and discussion

The prepared FTY720@SPION/PFP/RGD-NBs were black spheres with a diameter range of 160–220 nm, and there was no obvious mutual adhesion or local agglomeration between these nanobubbles (Fig. 1). The stability study showed that the prepared NBs did not change their sizes within 7 days at 4 °C, while their size increased by about 18% from day 1 to day 7 at 20 °C, as the average size expanded from 177.89 ± 6.14 nm to 210.51 ± 4.32 nm (Fig. 1C). The calculated average drug loading efficiency (LE) and encapsulation of efficiency (EE) of the FTY720@SPION/PFP/RGD-NBs were 9.18 ± 0.61% and 88.26 ± 2.31%, respectively, as listed in Table 2.

SPIONs are contrast agents for T2-weighted imaging in MRI, which have good biocompatibility and biodegradability. They can bind to hemoglobin and involve in the metabolic processes, avoiding accumulation in the body. Compared with other contrast agents, SPIONs have stronger MRI contrast enhancement effects, higher detection sensitivities, a large number of surface binding sites, and the ability to construct composite nanostructures for multi-mode imaging.[26,39–41] In this study,

Table 1 Primers used for qRT-PCR

Genes	Primer	Sequence
Caspase-9	Forward	5′-GCAGTAACCCCGAGCCAGATG-3′
	Reverse	5′-CCGGAGGAAATTAAAGCAACCAG-3′
Caspase-3	Forward	5′-TGCAGCAAACCTCAGGGAAA-3′
	Reverse	5′-TCACCATGGCTCAGAAGCAC-3′
p53	Forward	5′-GTGACACGCTTCCCTGGATT-3′
	Reverse	5′-GAGCTTCATCTGGACCTGGG-3′

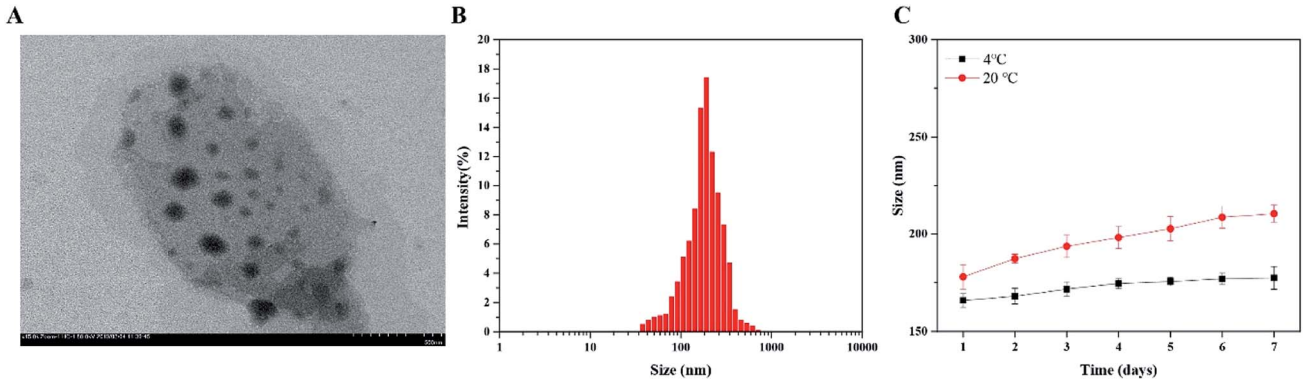

Fig. 1 Characterization of the FTY720@SPION/PFP/RGD-NB complex: (A) TEM image of the prepared NB complex, scale bar = 500 nm. (B) Size distribution of the prepared NB complex. (C) Size of the prepared NB complex changed with time (n = 7 days) at 4 °C and 20 °C.

SPIONs were prepared by a high-temperature pyrolysis method[37,38] and then encapsulated within NBs to achieve real-time MRI visualization.

The structure of SPIONs was confirmed by the XRD spectrum (Fig. S1†). The TEM image showed that the prepared SPIONs were spherical and monodisperse, with an average particle diameter of 8 nm and a PDI of 0.202 ± 0.012 (Fig. S2†). Magnetic response is one of the important performance indicators for testing magnetic materials, and hysteresis loops are used to characterize the responsiveness of magnetic materials to external magnetic fields. The profiles of hysteresis loops (Fig. 2) showed that the saturation magnetization (M_s) of SPIONs and FTY720@SPION/PFP/RGD-NBs was 59.9 emu g^{-1} and 19.95 emu g^{-1}, respectively. The hysteresis curves of all the samples passed through the origin, suggesting that the remanence was zero. This result indicated that the prepared SPIONs and NB complex were both superparamagnetic. Though the saturation magnetization of FTY720@SPION/PFP/RGD-NBs was lower than that of SPIONs, it showed good magnetic responsiveness to external magnetic fields and can be used for subsequent MRI studies.

The MRI T2WI scan results are shown in Fig. 2B. The images of first line were the water control group, and the images of second line were the prepared FTY720@SPION/PFP/RGD-NBs. As the concentration of SPIONs increased, the MRI image gradually darkened. This result suggested that the SPIONs in the prepared NBs complex could effectively reduce the T_2 relaxation time and enhance the MRI effects. In Fig. 2C, the transverse relaxation time T_2 of samples of different concentrations was obtained according to the scanned MRI T2 map. The reciprocal was plotted against the Fe concentration (mM) in the sample and linearly fitted to calculate the transverse relaxation rate of the sample R_2 (114.56 mM^{-1} s^{-1}). This result confirmed that the prepared FTY720@SPION/PFP/RGD-NBs had a high relaxation rate and T2WI scanning sensitivity conditions.

UTMD technology is a novel targeted drug or gene delivery method due to its non-invasive, safe, effective, and controllable characteristics. In this study, we used low-intensity focused ultrasound (LIFU) as the ultrasound trigger to burst the drug-loaded NBs, thereby improving the targeted deposition of the drug in the tumor tissues and reducing the toxic effects towards normal tissues. The *in vitro* release profiles of FTY720 from FTY720@SPION/PFP/RGD-NB with the promotion of LIFU were evaluated at pH 7.4 at 37 °C (Fig. 3). The amount of FTY720 released from the prepared NB complex was increased with the increase in the LIFU intensity. The corresponding drug release amount at 72 hours was 38.4 ± 1.1%, 58.7 ± 2.1%, 68.4 ± 3.0%, and 93.5 ± 2.9%, when the LIFU intensity was set to 0, 0.8, 1.6 and 2.4 W cm^{-2} respectively with an exposure time of 1 min. In addition, the samples with LIFU treatment showed a much faster release rate of FTY720 than the NBs without ultrasound exposure. At 12 h, FTY720 released by the sample treated with LIFU at 2.4 W cm^{-2}, 1.6 W cm^{-2} and 0.8 W cm^{-2} were 78.1 ± 2.4%, 56.4 ± 3.0% and 43.6 ± 2.4%, respectively. The amount of FTY720 released from the prepared NBs without the LIFU promotion was only 25.7 ± 1.4%. These results indicated that the selected LIFU intensity (2.4 W cm^{-2} with exposure time of 1 min) had the ability to burst the prepared NB complex and caused rapid drug release at the target site, which provided a basis for subsequent tumor treatment experiments.

To investigate HCC cell killing effect of FTY720@SPION/PFP/RGD-NBs with the combination of LIFU, we measured the viability of HepG2 and Huh7 cells treated with various NB complexes at different concentrations with or without ultrasound irradiation (Fig. 4a–d). For different concentrations of SPION/PFP/RGD-NBs, both HepG2 and Huh7 cell proliferations at 24 h and 48 h were all above 80%, indicating that the

Table 2 Characterizations of FTY720@SPION/PFP/RGD-NB at 20 °C

NBs	Zeta potential (mV)	EE (%)	LE (%)
FTY720@SPION/PFP/RGD-NBs	−38.00 ± 0.41	88.26 ± 2.31	9.18 ± 0.61%

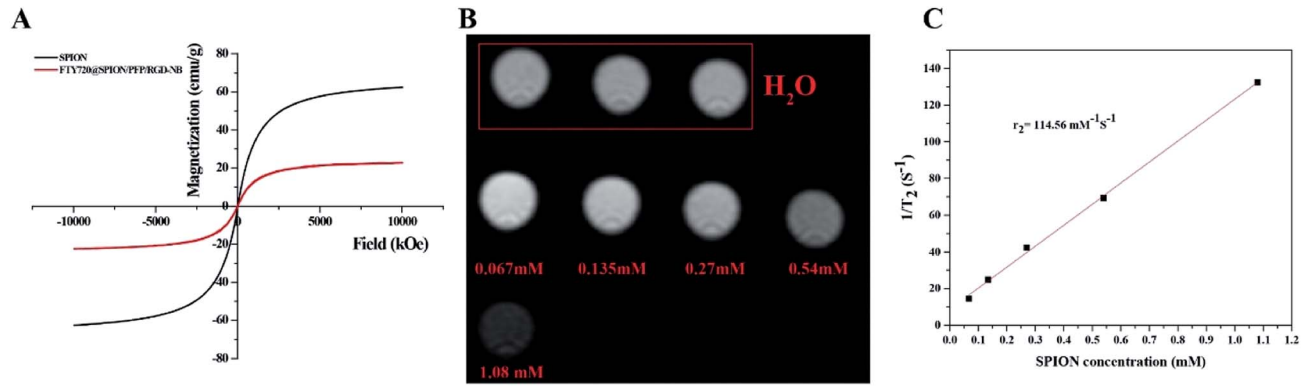

Fig. 2 *In vitro* MRI properties of the prepared NBs complex: (A) hysteresis loop of the prepared SPIONs and FTY720@SPION/PFP/RGD-NBs; (B) *in vitro* MRI images for FTY720@SPION/PFP/RGD-NBs of different concentrations scanned using a 3.0T MRI machine; and (C) plot of the transverse relaxivity R_2 of SPION.

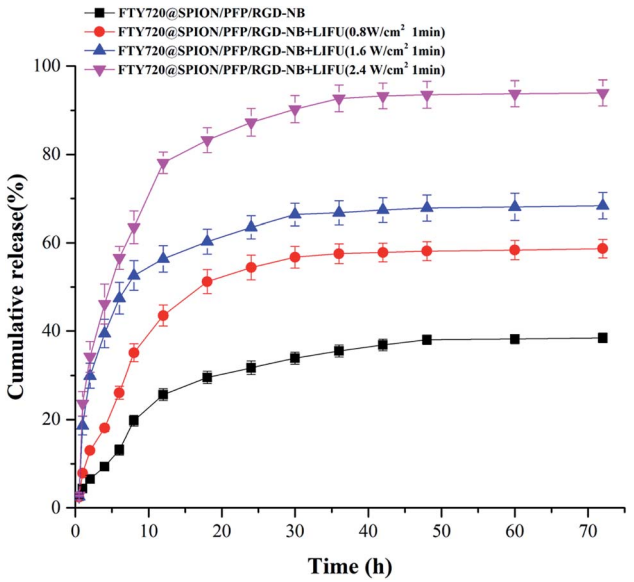

Fig. 3 *In vitro* release profiles of FTY720 from FTY720@SPION/PFP/RGD-NB complexes with or without the promotion of LIFU (output power of 0.8 1.6 or 2.4 W cm^{-2}, 1 MHz, duty cycle of 50% and an exposure time of 60 s) at 37 °C, pH 7.4.

prepared NB drug carrier has low toxicity to the cells. For the other FTY720-loaded NBs, the cytotoxicity showed a dosage-dependent manner. The higher the concentration of the drug-loaded NBs, the lower the cell viability. After ultrasound treatment, the HepG2 cells co-cultured with FTY720@SPION/PFP/RGD-NB (100 μg mL^{-1}) showed the lowest survival rate when compared to the other groups, which was only 15.21% and 14.71% at 24 h and 48 h, respectively. The Huh7 cells co-cultured with the FTY720@SPION/PFP/RGD-NB (100 μg mL^{-1}) showed similar trends (Fig. 4c and d), and the samples of FTY720@SPION/PFP/RGD-NB + LIFU (100 μg mL^{-1}) showed the lowest survival rate (35.21% and 28.18% at 24 h and 48 h, respectively) compared to the other groups. For both HepG2 and Huh7 cells treated with FTY720@SPION/PFP/NB + LIFU (*i.e.* non-RGD-targeted NBs + LIFU), the cell viability was lower than that for cells treated with FTY720@SPION/PFP/NB and FTY720@SPION/PFP/RGD-NB (*i.e.* RGD-targeted NBs) at 24 h. This might be due to the fact that the LIFU resulted in rapid drug (FTY720) release from the NBs within 24 h (as shown in Fig. 3), which would cause enhanced anti-tumor effects. Other studies in the literature also demonstrated with the ultrasound irritation could mediate the rapid drug release from liposomes and instantaneously change the permeability of cell membranes, leading to effective drug absorptions by tumor cells.[42,43]

To further investigate the cytotoxicity of the prepared NBs on normal cell lines, we performed CCK8 assay using normal fibroblast 3T3 cells co-cultured with the prepared NBs (Fig. 4e and f). The cell viability of 3T3 cells at both 24 h and 48 h were over 80% when NBs were equal or below 50 μg mL^{-1}; when NBs were set at a higher concentration of 100 μg mL^{-1}, the cell viability of 3T3 cells treated with FTY720@SPION/PFP/NB + LIFU or FTY720@SPION/PFP/RGD-NB + LIFU at 24 h decreased slightly to 78.14% and 76.27%, respectively; and the cell viability of these two samples at 48 h were 79.88% and 77.98%, respectively. The cell viability of 3T3 cells treated with other NBs at 100 μg mL^{-1} was all above 80%. These results suggested that the prepared NBs had good biocompatibility to health cell lines and had a higher targeting efficiency for HCC cells than normal fibroblast cells.

Effective intercellular uptake of drug-loaded NBs can enhance the therapeutic effects on cancer cells. By co-culturing with HepG2 cells *in vitro*, the targeting efficiency of the prepared drug-loaded NBs with or without ultrasound exposure (power 2.4 W cm^{-2}, 60 s) was evaluated using CLSM. As shown in Fig. 5, the cell nuclei were stained and indicated in blue, while the prepared NBs were indicated in red. For the cells with FTY720@SPION/PFP/NB (*i.e.* non-RGD-targeted group), there were very weak red fluorescence signals gathered around the cell membranes, while for the cells with FTY720@SPION/PFP/RGD-NB (*i.e.* RGD-targeted group), red fluorescence was clearly visible around the cell membranes. Combined with ultrasound exposure, both these two groups (*i.e.* FTY720@SPION/PFP/NB + LIFU and FTY720@SPION/PFP/RGD-

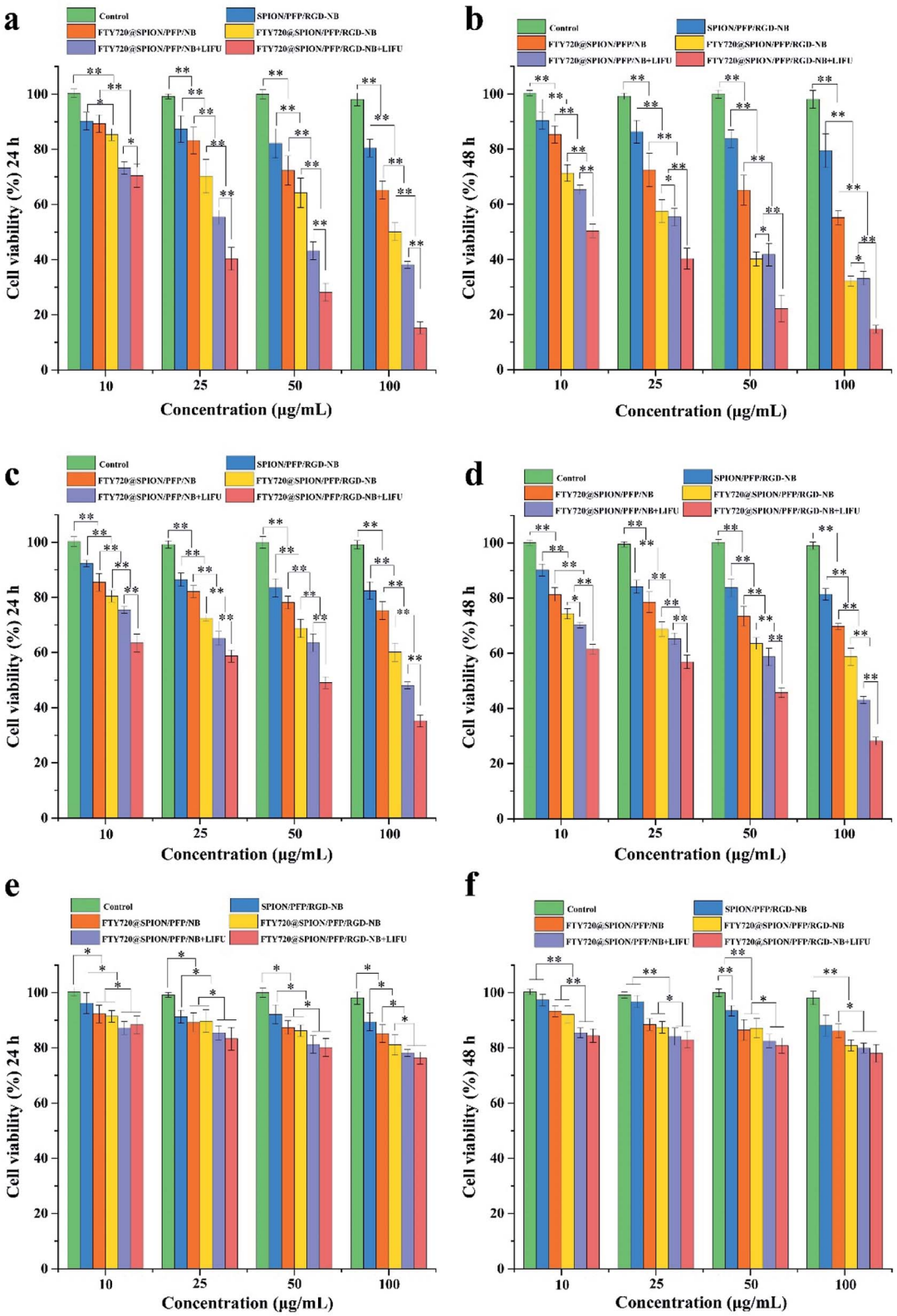

Fig. 4 Cell viability of different cells treated with various NB complexes at different concentrations and conditions (*$p < 0.05$, **$p < 0.01$): panels (a) and (b) were the cell viability of HepG2 cells co-cultured with the prepared NBs at 24 h and 48 h, respectively. Panels (c) and (d) were the cell viability of Huh7 cells cocultured with the prepared NBs at 24 h and 48 h, respectively. Panels (e) and (f) were the cell viability of 3T3 cells co-cultured with the prepared NBs at 24 h and 48 h, respectively.

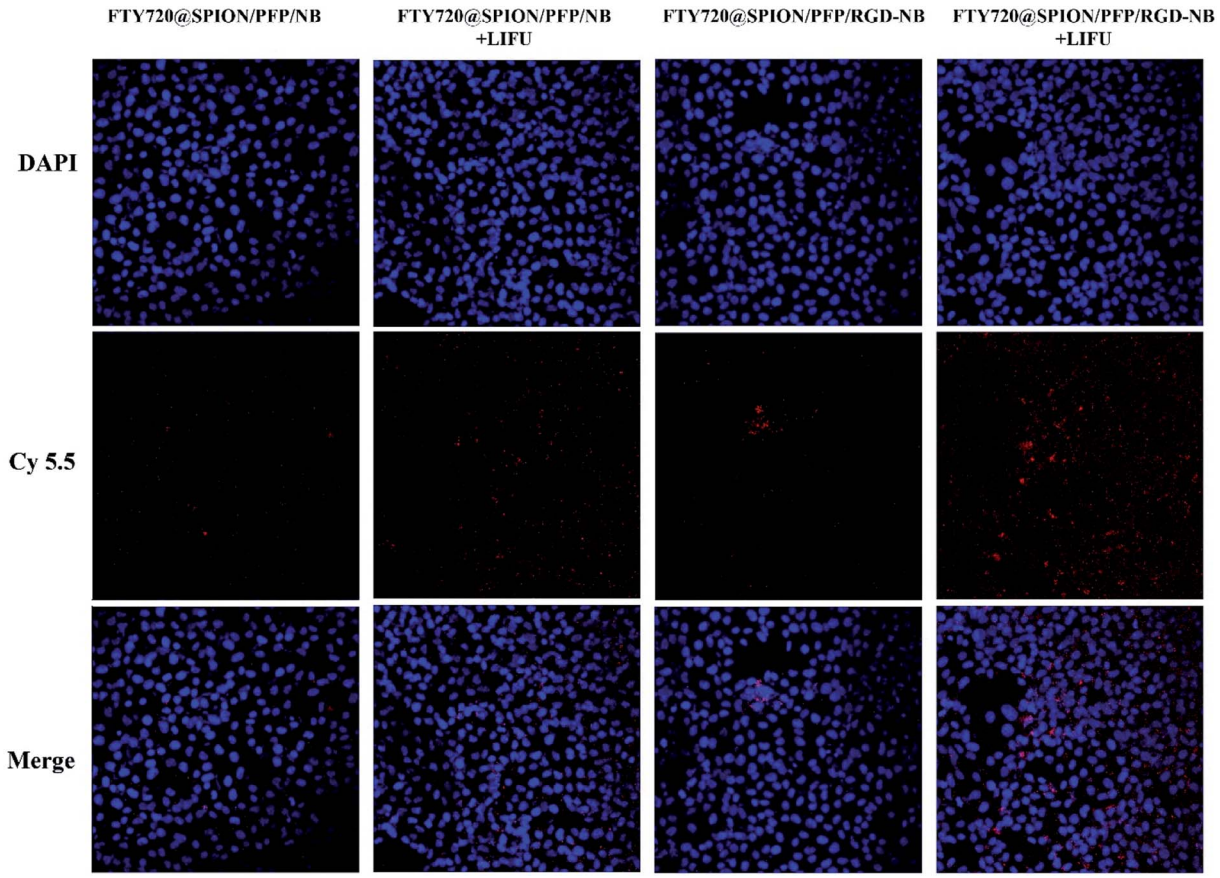

Fig. 5 Targeting efficiency of the prepared RGD-NBs with or without LIFU treatment: HepG2 cells were co-cultured with cy5.5-labelled FTY720@SPION/PFP/NBs or FTY720@SPION/PFP/RGD-NBs for 1 h.

NB + LIFU) showed enhanced red fluorescence signals around the cells, and the red signals for the RGD-targeted NBs + LIFU group were stronger than that of the non-RGD-targeted NBs + LIFU group. This might be due to the fact that the ultrasound irritation could cause cavitation effects and temporarily open the cell membranes. At the same time, the drug-loaded NBs were burst due to ultrasound irritation, and the drug could be effectively released from the collapsed NBs and accumulated in the tumor cells. Furthermore, the RGD peptide has been proved to have a high bind affinity to αvβ3 integrin, which was normally associated with various tumor cells.[44] A number of studies demonstrated that the RGD modified nano-drug delivery systems could improve the active targeting efficiency of tumor cells.[45–48] Thereby, the ultrasound irritation could mediate the drug-loaded NBs to be more easily internalized into the cells, and the prepared RGD-modified NBs could further improve cellular uptake and increase the delivery efficiency of FTY720.

The cellular uptake efficiency of the FTY720@SPION/PFP/NB or FTY720@SPION/PFP/RGD-NB was also evaluated by observing MRI T2-weighted imaging (T2WI) and by measuring T_2 value of HepG2 cells when incubated with different nanoparticles using a clinical 1.5T MRI scanner. As shown in Fig. 6, the T_2 value of the control group a (*i.e.* water) was highest, followed by the cells co-cultured with FTY720@SPION/PFP/NBs and FTY720@SPION/PFP/RGD-NBs without LIFU treatments (groups b and d). The T_2 values of the cells subjected to the LIFU treatment, *i.e.* group c (FTY720@SPION/PFP/NB + LIFU) and group e (FTY720@SPION/PFP/RGD-NB + LIFU), both showed a remarkable decrease compared to the control group a, and the T_2 value of group e (FTY720@SPION/PFP/RGD-NB + LIFU) was the lowest among all samples. These results indicated that with the assistance of LIFU treatment, the prepared NBs, *i.e.* FTY720@SPION/PFP/NBs and FTY720@SPION/PFP/RGD-NBs could be more effectively burst in the tumor area and showed an enhanced negative contrast in the corresponding MRI images. Group e showed about 0.67 times T_2 value of that of group c, suggesting that the RGD-equipped NBs might increase the cell absorption of the prepared NBs under the same conditions. This finding was consistent with the results of cellular targeting efficiency of the prepared RGD-NBs using CLSM (Fig. 5).

The mRNA expression levels of Caspase-3, Caspase-9 and p53 related to the apoptosis were detected by qRT-PCR assay. The results indicated that all the prepared NBs with or without LIFU treatment could increase the mRNA expression levels of Caspase-9, Caspase-3 and p53 when compared with the control group (Fig. 7). The sample with the highest mRNA expression levels was FTY720@SPION/PFP/RGD-NB + LIFU group. Tumors cells can increase the expression of anti-apoptotic genes, down-regulate the expression of apoptosis genes, and block the cell

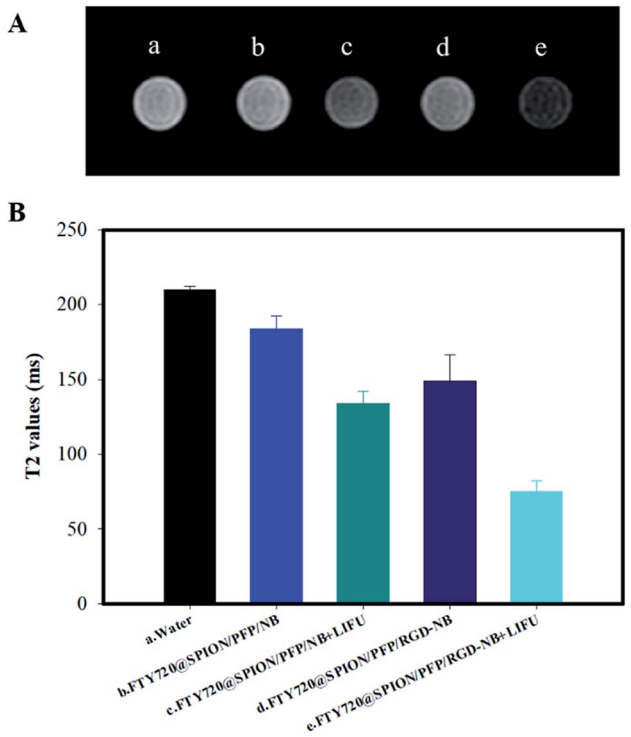

Fig. 6 Targeting efficiency of the prepared NBs under different conditions. Panel (A): T2WI images showed the signal intensity of HepG2 cells incubated with (a) water, (b) FTY720@SPION/PFP/NBs, (c) FTY720@SPION/PFP/NB + LIFUs, (d) FTY720@SPION/PFP/RGD-NBs, and (e) FTY720@SPION/PFP/NB + LIFUs. Panel (B): T_2 values of HepG2 cells incubated with the prepared NBs under different conditions.

death pathway at different levels of the apoptotic signal cascade reactions, thereby evading apoptosis to ensure survival of cancer cells. Apoptosis mainly goes through two pathways: death receptor pathway (exogenous pathway) and mitochondrial pathway (endogenous pathway).[49] The activation of either pathway will cause the protease to hydrolyze and activate the caspase family. Caspase-3 and Caspase-9 are the key molecules in the caspase family to execute and initiate cell apoptosis, playing vital roles in the process of cell apoptosis. p53 is one of the famous tumor suppressors in cells, and its expression can be enhanced by cytotoxic stress, resulting in cell cycle arrest and apoptosis. In this study, the expression levels of apoptosis-related mRNA Caspase-9, Caspase-3 and p53 were up-regulated in the HepG2 cells treated with various NBs. It is speculated that the prepared NBs could promote apoptosis of HepG2 cells. Combined with LIFU, the expression levels of these mRNA were higher than those without LIFU treatment, indicating that LIFU mediation might enhance these gene expressions.

4. Conclusions

In this study, we have successfully prepared an ultrasound-sensitive NB drug carrier, FTY720@SPION/PFP/RGD-NB, which showed good stability, high encapsulation efficiency and drug loading efficiency, and promoted the drug release rate under ultrasound mediation. *In vitro* MRI results confirmed that the prepared NB complex with SPIONs had a high relaxation rate and T2WI scanning sensitivity conditions. The study of cell viability suggested that FTY720@SPION/PFP/RGD-NB combined with LIFU has a significant proliferation inhibitory effect on HCC cells (HepG2 and Huh7 cells) and low toxicity to 3T3 cells. The cellular uptake study showed that the prepared FTY720@SPION/PFP/RGD-NB could effectively accumulate in the tumor cells with the promotion of LIFU. The qRT-PCR assay showed that LIFU-mediated FTY720@SPION/PFP/RGD-NB could significantly activate Caspase3, Caspase9 and p53 compared to the control group, inducing HepG2 apoptosis. These results together indicated that the prepared ultrasound-sensitive drug carrier (FTY720@SPION/PFP/RGD-NB) has a great potential to achieve the targeted delivery of sonodynamic treatment and provide a new strategy for tumor visualization through MRI.

Conflicts of interest

The authors declare no conflict of interest.

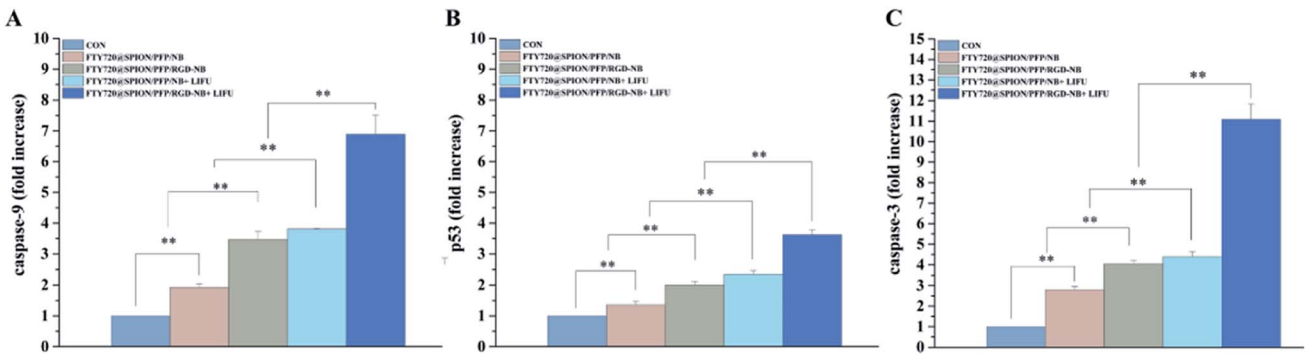

Fig. 7 mRNA expression levels of Caspase-9 (A), p53 (B) and Caspase-3 (C) in HepG2 cells. The cells were treated with the various prepared NBs with or without LIFU treatment for 48 h. The results are presented as mean ± SD from three independent experiments ($n = 3$), (*$P < 0.05$ and **$P < 0.01$).

Acknowledgements

Special fund for Science and Technology Development of Guangdong Province (direction of public welfare research and capacity building) 2016: experimental study on the transfection of human liver cancer HepG2 cells with ultrasound microvesicle mediated antisense miRNA-21/221 and miRNA-199a plasmids and the treatment of human liver cancer xenograft tumor in nude mice, no. 2016A020215015.

References

1 A. Chan, *et al.*, Transferability of Liver Transplantation Experience to Complex Liver Resection for Locally Advanced Hepatobiliary Malignancy - Lessons Learnt From 3 Decades of Single Center Experience, *Ann. Surg.*, 2020, DOI: 10.1097/SLA.0000000000004227.

2 R. Kloeckner, P. Galle and J. Bruix, Local and Regional Therapies for Hepatocellular Carcinoma, *Hepatology*, 2020, DOI: 10.1002/hep.31424.

3 G. Gunasekaran, *et al.*, Surgical Treatments of Hepatobiliary Cancers, *Hepatology*, 2020, DOI: 10.1002/hep.31325.

4 L. Chen, *et al.*, Pan-Asian adapted ESMO Clinical Practice Guidelines for the management of patients with intermediate and advanced/relapsed hepatocellular carcinoma: a TOS-ESMO initiative endorsed by CSCO, ISMPO, JSMO, KSMO, MOS and SSO, *Ann. Oncol.*, 2020, **31**(3), 334–351.

5 A. Craig, *et al.*, Tumour evolution in hepatocellular carcinoma, *Nat. Rev. Gastroenterol. Hepatol.*, 2020, **17**(3), 139–152.

6 X. Zhao, *et al.*, A Cleverly Designed Novel Lipid Nanosystem: Targeted Retention, Controlled Visual Drug Release, and Cascade Amplification Therapy for Mammary Carcinoma in vitro, *Int. J. Nanomed.*, 2020, **15**, 3953–3964.

7 K. Logan, *et al.*, Targeted chemo-sonodynamic therapy treatment of breast tumours using ultrasound responsive microbubbles loaded with paclitaxel, doxorubicin and Rose Bengal, *Eur. J. Pharm. Biopharm.*, 2019, **139**, 224–231.

8 Y. Sun, *et al.*, Tumor targeting DVDMS-nanoliposomes for an enhanced sonodynamic therapy of gliomas, *Biomater. Sci.*, 2019, **7**(3), 985–994.

9 H. Nesbitt, *et al.*, Gemcitabine loaded microbubbles for targeted chemo-sonodynamic therapy of pancreatic cancer, *J. Controlled Release*, 2018, **279**, 8–16.

10 L. Zhu, *et al.*, Peptide-Functionalized Phase-Transformation Nanoparticles for Low Intensity Focused Ultrasound-Assisted Tumor Imaging and Therapy, *Nano Lett.*, 2018, **18**(3), 1831–1841.

11 M. Li, *et al.*, Phase-shift, targeted nanoparticles for ultrasound molecular imaging by low intensity focused ultrasound irradiation, *Int. J. Nanomed.*, 2018, **13**, 3907–3920.

12 J. Correas, *et al.*, Diagnostic improvement of renal ultrasonography in humans after i.v. injection of perflenapent emulsion, *Acad. Radiol.*, 1998, S185–S188; discussion S199.

13 Y. Jing, *et al.*, Ultrasound-targeted microbubble destruction improved the antiangiogenic effect of Endostar in triple-negative breast carcinoma xenografts, *J. Cancer Res. Clin. Oncol.*, 2019, **145**(5), 1191–1200.

14 S. Tinkov, *et al.*, New doxorubicin-loaded phospholipid microbubbles for targeted tumor therapy: part I-formulation development and in vitro characterization, *J. Controlled Release*, 2010, **143**(1), 143–150.

15 P. Li, *et al.*, Ultrasound triggered drug release from 10-hydroxycamptothecin-loaded phospholipid microbubbles for targeted tumor therapy in mice, *J. Controlled Release*, 2012, **162**(2), 349–354.

16 E. VanBavel, Effects of shear stress on endothelial cells: possible relevance for ultrasound applications, *Prog. Biophys. Mol. Biol.*, 2007, **93**, 374–383.

17 F. Yuan, C. Yang and P. Zhong, Cell membrane deformation and bioeffects produced by tandem bubble-induced jetting flow, *Proc. Natl. Acad. Sci. U. S. A.*, 2015, **112**(51), E7039–E7047.

18 Y. Zhang, *et al.*, Docetaxel-loaded lipid microbubbles combined with ultrasound-triggered microbubble destruction for targeted tumor therapy in MHCC-H cells, *OncoTargets Ther.*, 2016, **9**, 4763–4771.

19 R. Kwekkeboom, *et al.*, Increased local delivery of antagomir therapeutics to the rodent myocardium using ultrasound and microbubbles, *J. Controlled Release*, 2016, **222**, 18–31.

20 R. Cavalli, A. Bisazza and D. Lembo, Micro- and nanobubbles: a versatile non-viral platform for gene delivery, *Int. J. Pharm.*, 2013, **456**(2), 437–445.

21 Y. Zhao, *et al.*, Glioma-targeted therapy using Cilengitide nanoparticles combined with UTMD enhanced delivery, *J. Controlled Release*, 2016, **224**, 112–125.

22 S. Sun, *et al.*, Applications of Micro/Nanotechnology in Ultrasound-Based Drug Delivery and Therapy for Tumors, *Curr. Med. Chem.*, 2020, DOI: 10.2174/0929867327666200212100257.

23 C. Liufu, *et al.*, Synergistic ultrasonic biophysical effect-responsive nanoparticles for enhanced gene delivery to ovarian cancer stem cells, *Drug Delivery*, 2020, **27**(1), 1018–1033.

24 J. Feshitan, *et al.*, Theranostic Gd(III)-lipid microbubbles for MRI-guided focused ultrasound surgery, *Biomaterials*, 2012, **33**(1), 247–255.

25 L. Li, *et al.*, Evaluation of microbubbles as contrast agents for ultrasonography and magnetic resonance imaging, *PLoS One*, 2012, **7**(4), e34644.

26 F. Yang, *et al.*, Superparamagnetic iron oxide nanoparticle-embedded encapsulated microbubbles as dual contrast agents of magnetic resonance and ultrasound imaging, *Biomaterials*, 2009, **30**, 3882–3890.

27 S. Spiegel and S. Milstien, The outs and the ins of sphingosine-1-phosphate in immunity, *Nat. Rev. Immunol.*, 2011, **11**(6), 403–415.

28 K. Chiba, FTY720, a new class of immunomodulator, inhibits lymphocyte egress from secondary lymphoid tissues and thymus by agonistic activity at sphingosine 1-

phosphate receptors, *Pharmacol. Ther.*, 2005, **108**(3), 308–319.

29 H. Azuma, *et al.*, Marked prevention of tumor growth and metastasis by a novel immunosuppressive agent, FTY720, in mouse breast cancer models, *Cancer Res.*, 2002, **62**(5), 1410–1419.

30 H. Azuma, *et al.*, Induction of apoptosis in human bladder cancer cells in vitro and in vivo caused by FTY720 treatment, *J. Urol.*, 2003, **169**(6), 2372–2377.

31 H. Omar, *et al.*, Antitumor effects of OSU-2S, a nonimmunosuppressive analogue of FTY720, in hepatocellular carcinoma, *Hepatology*, 2011, **53**(6), 1943–1958.

32 T. Lee, *et al.*, FTY720: a promising agent for treatment of metastatic hepatocellular carcinoma, *Clin. Cancer Res.*, 2005, **11**(23), 8458–8466.

33 C. Vicente, *et al.*, A novel FTY720 analogue targets SET-PP2A interaction and inhibits growth of acute myeloid leukemia cells without inducing cardiac toxicity, *Cancer Lett.*, 2020, **468**, 1–13.

34 C. Chua, *et al.*, Suppression of androgen-independent prostate cancer cell aggressiveness by FTY720: validating Runx2 as a potential antimetastatic drug screening platform, *Clin. Cancer Res.*, 2009, **15**(13), 4322–4335.

35 J. Camm, *et al.*, Cardiac and vascular effects of fingolimod: mechanistic basis and clinical implications, *Am. Heart J.*, 2014, **168**(5), 632–644.

36 N. Snelder, *et al.*, Characterization and Prediction of Cardiovascular Effects of Fingolimod and Siponimod Using a Systems Pharmacology Modeling Approach, *J. Pharmacol. Exp. Ther.*, 2017, **360**(2), 356–367.

37 S. Sun, *et al.*, Monodisperse MFe_2O_4 (M = Fe, Co, Mn) nanoparticles, *J. Am. Chem. Soc.*, 2004, **126**(1), 273–279.

38 Y. Qu, *et al.*, Enhanced magnetic fluid hyperthermia by micellar magnetic nanoclusters composed of Mn(x)Zn(1-x) Fe(2)O(4) nanoparticles for induced tumor cell apoptosis, *ACS Appl. Mater. Interfaces*, 2014, **6**(19), 16867–16879.

39 M. Shevtsov, *et al.*, Targeting experimental orthotopic glioblastoma with chitosan-based superparamagnetic iron oxide nanoparticles (CS-DX-SPIONs), *Int. J. Nanomed.*, 2018, **13**, 1471–1482.

40 X. Wang, *et al.*, Surface engineered antifouling optomagnetic SPIONs for bimodal targeted imaging of pancreatic cancer cells, *Int. J. Nanomed.*, 2014, **9**, 1601–1615.

41 M. Licciardi, *et al.*, Smart copolymer coated SPIONs for colon cancer chemotherapy, *Int. J. Pharm.*, 2019, **556**, 57–67.

42 Z. Gao, H. Fain and N. Rapoport, Ultrasound-enhanced tumor targeting of polymeric micellar drug carriers, *Mol. Pharmaceutics*, 2004, **1**(4), 317–330.

43 N. Rapoport, Z. Gao and A. Kennedy, Multifunctional nanoparticles for combining ultrasonic tumor imaging and targeted chemotherapy, *J. Natl. Cancer Inst.*, 2007, **99**(14), 1095–1106.

44 K. Temming, *et al.*, RGD-based strategies for selective delivery of therapeutics and imaging agents to the tumour vasculature, *Drug Resist. Updates*, 2005, **8**(6), 381–402.

45 Y. Liang, *et al.*, A Nanosystem of Amphiphilic Oligopeptide-Drug Conjugate Actualizing Both αvβ3 Targeting and Reduction-Triggered Release for Maytansinoid, *Theranostics*, 2017, **7**(13), 3306–3318.

46 X. Jiang, *et al.*, Self-assembled peptide nanoparticles responsive to multiple tumor microenvironment triggers provide highly efficient targeted delivery and release of antitumor drug, *J. Controlled Release*, 2019, **316**, 196–207.

47 I. Ullah, *et al.*, Nose-to-Brain Delivery of Cancer-Targeting Paclitaxel-Loaded Nanoparticles Potentiates Antitumor Effects in Malignant Glioblastoma, *Mol. Pharmaceutics*, 2020, **17**(4), 1193–1204.

48 H. Ruan, *et al.*, Stapled RGD Peptide Enables Glioma-Targeted Drug Delivery by Overcoming Multiple Barriers, *ACS Appl. Mater. Interfaces*, 2017, **9**(21), 17745–17756.

49 I. Verbrugge, R. Johnstone and M. Smyth, SnapShot: extrinsic apoptosis pathways, *Cell*, 2010, **143**(7), 1192.

